



Adaptive removal of time-varying harmonics for chatter detection in thin-walled turning

Longyang Ding¹ · Yuxin Sun¹ · Zhenhua Xiong¹

Received: 9 April 2019 / Accepted: 20 September 2019 / Published online: 23 November 2019
© Springer-Verlag London Ltd., part of Springer Nature 2019

Abstract

Chatter is a kind of undesired vibration with multiple adverse effects in machining operations, and online detection of chatter is crucial for chatter avoidance or suppression. However, it is observed that time-varying harmonic components are abundant in turning of thin-walled parts. The emergence of harmonics alters conventional frequency distribution patterns of the measured signal. In particular, it is a very challenging task to detect chatter in an early stage when the signal spectrum is dominated by the harmonics. This paper firstly investigates theoretically the relationship between the chatter frequency and the natural frequency based on a well-accepted chatter model of turning. The chatter frequency is found to vary far more slowly than the natural frequency during the thin-walled turning. Based on this finding, the adaptive signal predictor is proposed as a preprocessor for chatter detection, which can alleviate harmonics interference and noise with no prior knowledge of the workpiece dynamics. Furthermore, an improved adaptive filter algorithm is developed to enhance the performance of time-varying harmonics removal. Finally, simulation and experimental results validate the effectiveness of the proposed approach in harmonics removal and noise reduction for chatter detection in thin-walled turning.

Keywords Chatter detection · Harmonics removal · Adaptive filter · Thin-walled parts

1 Introduction

The self-excited chatter is a kind of unstable vibration phenomenon commonly encountered in machining. Furthermore, chatter vibration results in numerous adverse effects, including harm to machine tools, deteriorated surface quality, harsh noise, and waste of material and energy. The complicated mechanism and elusive behavior make it very difficult to fully understand and completely avoid chatter in machining [1]. To achieve high productivity, some researchers have focused on chatter prediction based on stability lobe diagrams [2], which guide the selection of cutting parameters for chatter-free machining. But it is usually difficult to use this approach to avoid chatter in industrial practice due to inevitable model errors and uncer-

tainties [3, 4]. Another approach is to automatically identify the machining status and suppress chatter [5, 6], which is proved to be useful and reliable. In particular, it is desirable to detect or predict chatter timely and accurately in order to minimize the adverse effects caused by chatter vibration.

Due to the requirement of lightweight design in various fields of industrial manufacturing, the proportion of thin-walled parts raises quickly [7]. However, their low stiffness and massive material removal easily cause machining chatter, which has been one of the most challenging problems in both the industrial and the academic communities. Mehdi et al. [8] investigated the dynamic behavior of a thin-walled cylindrical workpiece in turning. Khoshdarregi and Altintas [9] found that instantaneous shell deformations due to the cutting forces caused residual shell vibrations, which could affect the chip thickness when the corresponding point arrived at the cutting region. Liu et al. [10] proposed a varying threshold for chatter detection to identify chatter in milling of thin-walled workpieces by monitoring the cutting torque. Harmonic filters were used to remove the current harmonics induced by the cutting force measurement system. Urbikain et al. [11] observed that the cutting frequency and its multiples appeared under stable and unstable conditions in

✉ Zhenhua Xiong
mexiong@sjtu.edu.cn

¹ State Key Laboratory of Mechanical System and Vibration, School of Mechanical Engineering, Shanghai Jiao Tong University, Shanghai 200240, China

turning using the discrete Fourier transform (DFT) of the force signal.

Many approaches have been proposed for chatter detection during the past decades. The extensive literature review shows that there are mainly four types of techniques for chatter detection, namely, time domain or frequency domain analysis, time-frequency domain analysis, pattern recognition, and others [12]. When chatter occurs, the amplitude of vibrational signals is increasing significantly. Thus some features can be extracted from time-domain signals to indicate chatter, such as once per revolution sampling [13]. From the frequency spectrum point of view, there is a trend to transform energy from broadband to narrowband in the development process of chatter. This characteristic in the frequency domain is utilized to detect chatter, such as fast Fourier transform (FFT) [14]. Time-frequency domain analysis, for example, wavelet transform (WT) [15], was applied to analyze the frequency components with varying resolutions. Pattern classification methods, such as the support vector machine [16], was also proposed in chatter detection. Except for the above signal processing methods, many chatter indicators are derived from statistics theory, like energy entropy [17]. Since the harmonics of the natural frequency in turning of flexible parts mainly affect the frequency spectrum of monitoring signals, the chatter detection methods related to the frequency spectrum distribution will be strongly influenced by the harmonics interference.

As a matter of fact, harmonics often present in milling, which is caused by the forced vibration of the tool. Because the milling tool intermittently enters and leaves the workpiece during the milling, the frequencies of forced vibration are integer multiples of the spindle frequency. In contrast, the tool tip contacts the workpiece continually in turning. Therefore, the harmonics are mainly determined by the thin-walled workpiece dynamics in the turning process, and their frequencies are evidently time-varying due to material removal. Thus, the comb filter used to filter out harmonics in milling [18] cannot work in thin-walled turning. Besides, the natural frequency of the thin-walled workpiece needs to be obtained in advance by modal tests if the band-pass filter is used for harmonics removal. There is still no practical solution to the harmonics removal for chatter detection in turning of flexible workpieces.

To solve this problem, the adaptive signal predictor is introduced to filter out the time-varying harmonics in turning of thin-walled parts in this paper. By theoretical analysis, we discover that the chatter frequency varies more slowly than the natural frequency in thin-walled turning. Therefore, their differences in autocorrelation can be utilized to alleviate the harmonics interference. Moreover, an improved normal least mean square (NLMS) algorithm is proposed for the adaptive signal predictor to enhance the

filtering ability. In this way, no prior knowledge is required to remove harmonics for chatter detection when turning thin-walled parts.

The remainder of this paper is arranged as follows. Section 2 presents the encountered problem for chatter detection in turning of thin-walled workpieces and investigates the frequency variation during chatter. In this section, the relationship between the chatter frequency and the natural frequency of a thin-walled disc is investigated theoretically in the end-face turning. Moreover, their relative rates of change are revealed quantitatively. Section 3 proposes the adaptive signal predictor with an improved NLMS algorithm to separate signals with big differences in the rate of frequency change, which is verified by simulation. In Section 4, the effectiveness of the adaptive signal predictor in alleviating the interference of harmonics and noise is experimentally confirmed. Finally, conclusions are drawn in Section 5.

2 Problem formulation and frequency analysis

Due to high flexibility and varying dynamics, there is a significant difference between the turning process of a flexible workpiece and that of a relatively rigid workpiece. Further, this difference brings about new problems for the existing chatter detection approaches. In this section, the phenomenon that the harmonics of the natural frequency emerge in the chatter signal is exposed and its consequences on chatter detection are pointed out. Then the change characteristics of the natural frequency and the chatter frequency are investigated using a well-accepted chatter model in turning, which provides guidance for harmonics removal.

2.1 Problem formulation

As mentioned above, chatter vibration presents a challenge to achieve high dimensional accuracy and productivity in turning of thin-walled parts. On-line detection is very essential to avoid chatter. Various signals have been utilized to monitor the machining state, such as the cutting force, audio signals, and vibration. The sampled signal in the chatter-free state is generally deemed to obey a Gaussian distribution. While chatter has fully developed, the monitoring signal is depicted as a harmonic function with a single frequency. To achieve a unified representation, the signal is modeled as a single sinusoid signal added to random noise [19], namely,

$$a(t) = A \sin(\omega t) + \text{rand}(t) \quad (1)$$

where t denotes time, $a(t)$ and $\text{rand}(t)$ are the sampled signal and the random function representing signals in the chatter-free state, respectively, ω is the angular chatter frequency and A is the amplitude of the chatter frequency component. A is increasing during the development of chatter. The sampled signal is random noise in the stable state, while A is large and $a(t)$ approximately equals a sinusoid signal in the chatter state. From the energy distribution point of view, chatter results in energy aggregation around the chatter frequency, which leads to the decreased uniformity of energy distribution. Many chatter detection methods are based on this change in signal characteristics, such as the wavelet packet entropy (WPE) [20].

However, when it comes to the turning of thin-walled workpieces with low stiffness, high-order vibration modes are very prone to be excited even in the stable state. Moreover, multiple mode frequencies of thin-walled parts are often low and close to each other. Therefore, they may well be aroused by the cutting force and the monitoring signal would contain multiple mode frequencies. As a result, the harmonics and inter-harmonics of multiple mode frequencies dominate the energy spectrum of monitoring signals in the stable and transition state, which is different from the conventional energy distribution pattern. On the other hand, chatter actually experiences a premature process, namely, the transition stage, before it has fully developed [21]. Moreover, there are no obvious chatter marks on the machined surface at the transition stage. Therefore, chatter is expected to be recognized at this stage so that damage incurred by chatter can be mitigated as much as possible. The signal characteristics in transition state are very critical to chatter detection at the early stage. However, the existing approach for chatter detection may be nullified due to the emergence of harmonics in turning of thin-walled parts.

2.2 Frequency analysis

In order to filter out harmonics, the frequency characteristics of signals in turning of thin-walled workpieces should be firstly investigated. The turning process of the flexible workpiece is impractically complex due to location-dependent modal parameters and material removal. Moreover, the flexible workpieces in turning are characterized by various geometrical shapes, such as a long slender bar, a thin-walled circular cylindrical shell, and a thin-walled disc. Besides, the boundary conditions are also difficult to elaborate. As a result, the modeling of machining chatter in turning of flexible parts becomes very challenging. Until today, several models have been proposed for the specific type of flexible workpieces. Stepan et al. modeled the varying dynamic properties of a long slender work-

piece due to the material removal process using the finite element method [22]. Chanda and Dwivedy studied simultaneously the nonlinear dynamics of the tool and the thin cylindrical workpiece for turning operations [23]. Guo et al. developed a time-varying distributed-parameter model for the dynamics of a rotating thin-walled plate [24]. Although the above-mentioned models were demonstrated to have a certain degree of validity by comparisons between the predicted and experimental stability boundaries, they either need to acquire modal parameters of each position on the flexible workpiece or depend on finite element analysis, which is difficult to implement in industrial production.

It is noted that modal parameters of thin-walled parts change remarkably during the turning process due to material removal. Therefore, the chatter frequency varied according to the natural frequency of a thin-walled workpiece [22]. Although the cutting force is influenced by many nonlinear factors, such as process damping, the linearized model has been extensively accepted [5, 25, 26] and utilized to predict the chatter frequency with adequate precision in the orthogonal turning [27]. In this paper, the well-accepted chatter model in Fig. 1 [28] is employed to approximately model the dynamics of the turning process with flexible workpieces and to derive the relationship between the natural and chatter frequency to some extent. In this model, the workpiece is modeled as a single-degree-of-freedom body since the thin-walled disc in the direction perpendicular to the plate has a much lower stiffness than the other two directions. Moreover, it is reasonable to assume that the tool is rigid with respect to the flexible workpiece. The modal parameters of the flexible workpiece are approximated as constants within one cut. For this cutting model, the linearized cutting force $F_f(t)$ can be expressed as

$$F_f(t) = K_f a h(t) = K_f a [h_0 - (x(t) - x(t - T))] \quad (2)$$

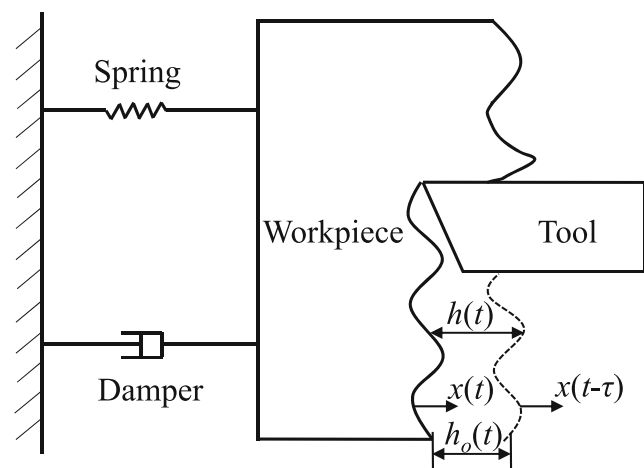


Fig. 1 Mechanism of regenerative chatter in the turning operation with the flexible workpiece

where t is the time, T is the delay time, K_f is the cutting force coefficient in the direction of feed, a is the depth of cut, $h(t)$ and h_0 are the dynamic cutting thickness and the nominal cutting thickness, respectively, $x(t)$ and $x(t - T)$ denote the current displacement and the previous displacement, respectively. When the amplitude of chatter vibration is too large (i.e., $x(t) - x(t - T) > h_0$), the tool jumps out of cut, which produces a zero chip thickness and zero cutting force. As a result, the whole process is too complex and nonlinear to model correctly analytically. Such severe chatter for a long time is always not allowed. Therefore, the influence of the tool jumping out of cut is neglected. For a single-degree-of-freedom system, the governing equation of motion is represented as

$$m\ddot{x}(t) + c\dot{x}(t) + kx(t) = F_f(t) \quad (3)$$

where m is the modal mass of the workpiece, and c and k are the structural damping coefficient and structural stiffness, respectively. In the Laplace S-domain, the dynamic cutting thickness $h(t)$ can be expressed as

$$h(s) = h_0 + \left(e^{-sT} - 1\right)x(s). \quad (4)$$

The Laplace transform function of this system is defined as

$$\Phi(s) = \frac{x(s)}{F_f(s)} = \frac{\omega_n^2}{ks^2 + 2\xi\omega_n s + \omega_n^2} \quad (5)$$

where ω_n is the angular natural frequency of the workpiece and ξ is the damping ratio. The current vibration displacement of the workpiece is given as

$$x(s) = F_f(s)\Phi(s) = K_f ah(s)\Phi(s). \quad (6)$$

Substituting Eq. 6 into Eq. 4, another form of $h(s)$ is expressed as

$$h(s) = h_0 + \left(e^{-sT} - 1\right) K_f ah(s)\Phi(s). \quad (7)$$

The stability of this closed-loop transfer function is determined by the roots of its characteristic equation, which is derived as

$$1 + \left(1 - e^{-sT}\right) K_f a \Phi(s) = 0. \quad (8)$$

When the real part of the characteristic root equals zero, the system is critically stable. The characteristic root now becomes $j\omega_c$, where j is an imaginary unit and ω_c is the angular chatter frequency. Subsequently, the characteristic equation becomes

$$1 + \left(1 - e^{-sT}\right) K_f a_{\text{lim}} \Phi(j\omega_c) = 0 \quad (9)$$

where a_{lim} is the critical depth of cut. If $\Phi(j\omega_c)$ is divided into a real part and an imaginary part, namely,

$$\Phi(j\omega_c) = G + jH. \quad (10)$$

Substituting Eq. 10 into Eq. 9 and splitting the real and imaginary part, Eq. 9 can be rewritten as

$$\begin{aligned} & \{1 + K_f a_{\text{lim}} [G(1 - \cos \omega_c T) - H \sin \omega_c T]\} \\ & + j \{G \sin \omega_c T + H(1 - \cos \omega_c T)\} = 0. \end{aligned} \quad (11)$$

According to Eq. 11, the real and imaginary parts of the characteristic equation have to be zero. It is considered that the imaginary part equals zero, namely,

$$G \sin \omega_c T + H(1 - \cos \omega_c T) = 0. \quad (12)$$

When the phase of Φ is represented by Ψ , according to Eq. 12

$$\tan \Psi = \frac{H(\omega_c)}{G(\omega_c)} = \frac{\sin \omega_c T}{\cos \omega_c T - 1} = \tan \left(\frac{\omega_c T}{2} - \frac{3\pi}{2} \right). \quad (13)$$

Then the relation between Ψ and ω_c can be deduced:

$$\omega_c T = 2\Psi + (3 + 2k)\pi \quad (14)$$

where k is the number of vibration cycles. Substituting the characteristic root into Eq. 5, Φ can be further expressed as

$$\Phi(j\omega_c) = \frac{1}{k \left(1 - \frac{\omega_c^2}{\omega_n^2} + j \frac{2\xi\omega_c}{\omega_n} \right)}. \quad (15)$$

If we set $r = \omega_c/\omega_n$ and split up the real and imaginary parts of $\Phi(j\omega_c)$, simplified results are

$$G = \frac{1 - r^2}{k \left[(1 - r^2)^2 + (2\xi r)^2 \right]}, \quad (16)$$

$$H = \frac{-2\xi r}{k \left[(1 - r^2)^2 + (2\xi r)^2 \right]}. \quad (17)$$

Therefore, the phase of the transfer function is calculated as

$$\Psi = \arctan \frac{H}{G} = \arctan \frac{2\xi r}{r^2 - 1}. \quad (18)$$

Substituting Eq. 18 into Eq. 14, the relation between ω_c and ω_n is

$$\tan \frac{\omega_c T - 3\pi}{2} = \frac{2\xi\omega_c\omega_n}{\omega_c^2 - \omega_n^2}. \quad (19)$$

In addition, T is the time taken for one revolution which is calculated by $60/n$, where n in r/min is the spindle speed. Finally, the relation between the chatter frequency f_c and the natural frequency f_n is presented as

$$\tan \frac{\frac{120\pi f_c}{n} - 3\pi}{2} + \frac{2\xi f_c f_n}{f_n^2 - f_c^2} = 0. \quad (20)$$

It has been demonstrated that natural frequencies of workpieces are not sensitive to low spindle speeds, but they decrease linearly with the part thickness [24]. Therefore, the natural frequencies of the thin-walled workpiece are remarkably time-varying in turning processes. To investigate the relationship between the natural and chatter frequency, the model parameters in ref. [29] are adopted. The corresponding parameters are $n = 758.15$ r/min and $\xi = 0.0105$. According to Eq. 20, f_c as a function of f_n ranging from 200 to 900 Hz is shown in Fig. 2, since natural frequencies of thin-walled parts are often low. It is noted that the slope of the curve k_{cn} , which represents the rate of relative change between f_c and f_n , is always less than 1. Moreover, k_{cn} is gradually increasing with f_n and far less than 0.5 in most cases. In Fig. 2, k_{cn} at two sample points are 0.182 and 0.318, respectively. It is found that the chatter frequency varies far more slowly than the natural frequency in turning of thin-walled discs.

It is seen in Eq. 20 that ξ and n are two key parameters. Therefore, their effects on k_{cn} should be studied. For the sake of simplification, k_{cn} is approximately replaced by the quotient, which the relative change of f_c is divided by that of f_n in a small range. The chatter frequency of 822 Hz is adopted from Experiment 1 in Section 5. Considering that the chatter frequency changes from 822 to 823 Hz, the corresponding k_{cn} is calculated for various spindle speeds and damping coefficients. k_{cn} as a function of ξ and n is fitted with the quadratic interpolation method and shown in Fig. 3. It can be seen that k_{cn} increases with the decrease of ξ and the increase of n . In addition, we can see that k_{cn} is always less than 0.5 in the range of low spindle speeds. In practice, the damping ratio of a thin-walled workpiece is usually greater than 0.01 [9, 30]. Therefore, it is confirmed that the chatter frequency varies more slowly than the natural frequency during the turning of thin-walled workpieces.

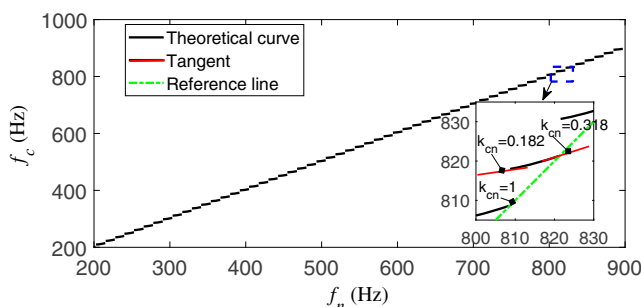


Fig. 2 Behavior of the chatter frequency varies with respect to the natural frequency of the thin-walled part in ref. [29]

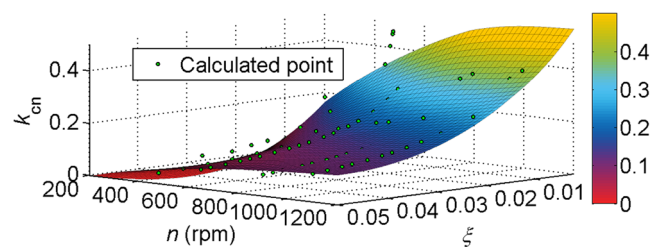


Fig. 3 Effects of n and ξ on k_{cn}

3 Adaptive harmonics removal approach

With the development of computing capability and emerging algorithms, the adaptive filter has been successfully used in various applications such as system identification, noise canceling, and echo cancellation. In order to separate noise and periodic signals, the adaptive signal predictor based on the difference in autocorrelation is proposed [31]. Actually, signals with different rates of frequency change also have a difference in autocorrelation. Therefore, we attempt to utilize this difference to weaken effects of the harmonics interference and improve the adaptive signal predictor.

3.1 Adaptive signal predictor

Based on signal correlation, the adaptive signal predictor is an application of the adaptive filter in noise canceling. It is assumed that the input of an adaptive signal predictor is composed of a random and a periodic signal, namely,

$$x(t) = x_0(t) + N(t) \tag{21}$$

where $x_0(t)$ and $N(t)$ denote the periodic signal and the random signal, respectively. The autocorrelation function of $x(t)$ is defined as $R_x(\tau)$, which is expressed as

$$R_x(\tau) = \lim_{T \rightarrow \infty} \frac{1}{T} \int_0^T x(t)x(t + \tau) dt \tag{22}$$

where τ is the delay time. The random signal $N(t)$ and $N(t + \tau)$ have no correlation with $x_0(t)$ and $x_0(t + \tau)$. Therefore, correlation coefficients among them equal zero. Substituting Eq. 21 into Eq. 22, the simplified $R_x(\tau)$ is derived as

$$R_x(\tau) = R_{x_0}(\tau) + R_N(\tau) \tag{23}$$

where $R_{x_0}(\tau)$ and $R_N(\tau)$ denote the autocorrelation function of $x_0(t)$ and that of $N(t)$, respectively. With long

delay time, $R_N(\tau)$ is close to zero but $R_{x_0}(\tau)$ remains unchanged.

Based on signal delay and the adaptive filter, the basic adaptive signal predictor system is depicted in Fig. 4. In Fig. 4, a wide-band signal $n(i)$ and a periodic signal $p(i)$ constitute the desired signal $d(i)$ and its delayed version is served as the adaptive filter input. The delay time makes the wide-band signal lose correlation with its delayed version, but the correlation between the periodic signal and its delayed version remains strong. As the output of the adaptive filter, an optimum estimate of the periodic signal $y(i)$ is obtained after iteratively adjusting weight coefficients. Then the wide-band signal is extracted as the error signal $e(i)$ by signal subtraction. The natural frequency component has weak autocorrelation through time delay due to a large rate of frequency change. In contrast, the chatter frequency component with a small rate of frequency change shows strong autocorrelation via time delay. Therefore, the chatter frequency component is isolated by the adaptive signal predictor.

3.2 Improved NLMS algorithm

Recently, various algorithms have been proposed to adjust automatically and iteratively weights of the adaptive filter in order to minimize a prescribed criterion [32, 33]. The least mean square (LMS) is the most frequently used search algorithm in the adaptive filtering due to its computational simplicity. The instantaneous estimate of the gradient is employed to search the minimum mean square error (MSE) in the LMS algorithm. The LMS algorithm with a single input can be represented as [34]

$$y(i) = \omega^T x(i) = \sum_{k=0}^{N-1} \omega_k(i) x_k(i) \quad (24)$$

$$e(i) = d(i) - y(i) \quad (25)$$

$$\omega(i+1) = \omega(i) + \mu e(i) x(i) \quad (26)$$

where $\omega(i)$ is the filter coefficient vector at instant i , $x(i)$ and $y(i)$ denote the input and output of the adaptive filter, respectively, N is the filter order, $e(i)$ is the estimation error of the adaptive filter, $d(i)$ represents the desired signal, and

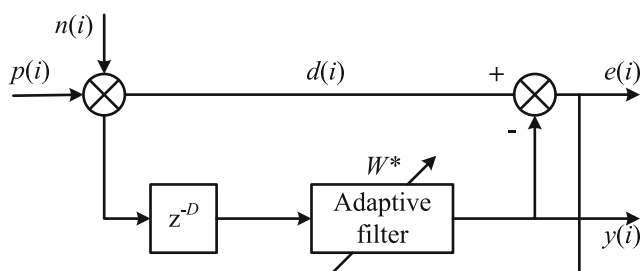


Fig. 4 Block diagram of the adaptive signal predictor

μ is the fixed step size. The convergence rate and stability of the algorithm are controlled by the step size, which is constrained by

$$0 < \mu < \frac{1}{\lambda_{\max}} \quad (27)$$

where λ_{\max} is the maximum eigenvalue of the autocorrelation matrix of the input signal.

That the weight increment is proportional to the input vector makes the LMS algorithm sensitive to the scaling of its input, and gradient noise is amplified. Therefore, it is very difficult to select a proper step size that keeps a balance between stability and accuracy. To overcome this difficulty, the NLMS algorithm is proposed with a normalized step size independently by Nagumo (1967) and Albert (1967), which is written as

$$\mu(i) = \frac{\mu_0}{\delta + x^T(i)x(i)} \quad (28)$$

where μ_0 is the convergence factor and δ is a small positive constant in case that the denominator becomes zero. In the NLMS algorithm, μ_0 is a key parameter associated with the step size and Paulo et al. have studied its available range [35], which is given as: $0 < \mu_0 < 2$. With a large step size, the rate of convergence is fast but the increased MSE and the instability of the algorithm are encountered, and vice versa. Therefore, the selection of μ_0 needs to consider both the MSE and the rate of convergence. In most cases, the value of μ_0 should not be chosen close to the upper bound due to the approximations and assumptions made.

The LMS algorithm is still far from the optimum trade-off between the steady-state misadjustment and the convergence rate. To overcome this deficiency, various variable step-size LMS algorithms have been proposed [36]. By contrast, the NLMS algorithm is regarded as the best one when considering the ease of use, computational complexity, and performance. However, the convergence factor in the NLMS algorithm is constant. To produce a smaller MSE as fast as possible, an improved NLMS algorithm is developed in this paper by defining a variable convergence factor as

$$\mu_0(i) = \alpha \left(1 - \frac{1}{|e(i)e(i-I)| + 1} \right) \quad (29)$$

where α is a constant, I as the delay factor is a positive integer greater than 1. The value scope of $\mu_0(i)$ is controlled by α , which plays the same role as μ_0 in the NLMS algorithm. Therefore, the selection method for an appropriate μ_0 can be directly applied to determining α . A large delay factor promotes the attenuation of the autocorrelation of the component with a larger rate of frequency change. Thus, I requires to be adjusted according to the attenuation degree of the autocorrelation of components with larger rates of frequency change.

The step size adjustment is connected to the autocorrelation of errors in order to weaken aperiodic signals. Moreover, the convergence factor defined in Eq. 29 produces an increasing resolution for searching the minimum MSE due to error reduction. Therefore, faster convergence and reduced MSE are achieved simultaneously by the proposed algorithm. In conclusion, the improved NLMS algorithm retains the advantages of the NLMS algorithm and enhances the filtering ability.

4 Simulation results

It has been extrapolated that the adaptive signal predictor can remove signal components with very weak periodicity. To verify the above analysis, simulations were carried out with a composite signal, which contained two components with linearly increasing frequencies and random noise and was expressed as

$$s(t) = \sin(4\pi t + \pi t^2) + \sin(4\pi t + 0.2\pi t^2) + \text{rand}(t). \quad (30)$$

$N = 5$ and $D = 50$ were selected in the adaptive signal predictor. Moreover, the NLMS algorithm with $\mu_0 = 0.0005$ and the improved NLMS algorithm with $I = 1$ and $\alpha = 0.0005$ were applied in the adaptive filter. Besides, the time-frequency analysis technique is required to demonstrate simulation results. In this paper, the short-time Fourier transform (STFT) was utilized to give the time-frequency distribution of the simulated signal and its output via the NLMS and improved NLMS adaptive filter in Fig. 5.

Figure 5a shows the time-frequency distribution of the original composite signal, and each component has the same energy. Compared with Fig. 5a, most of random noise is removed in Fig. 5b. Moreover, the remaining energy for the signal with the slope of frequency change $k_f = 1$ in Fig. 5b is 28.2% of the one with $k_f = 0.2$ after being processed by the NLMS adaptive filter. The similar comparison is made when the improved NLMS algorithm is applied, and the corresponding percentage is only 12.57%. In the simulation, the signal with $k_f = 0.2$ preserves 76.73% and 52.06% of its original energy via the NLMS and improved NLMS filter, respectively. Although the improved NLMS filter removes more signal energy than the NLMS filter, it can produce a bigger difference in remaining energy for signals with various rates of frequency change. In the simulation, the ratio of the remaining energy of the signal with the slope of the frequency change $k_f = 0.2$ to that with the slope of frequency change $k_f = 1$ increases from 2.72 to 4.14 when the improved NLMS algorithm is utilized in the adaptive signal predictor to replace the NLMS algorithm. Therefore, those signal components with much larger rates of frequency change can be thought to be

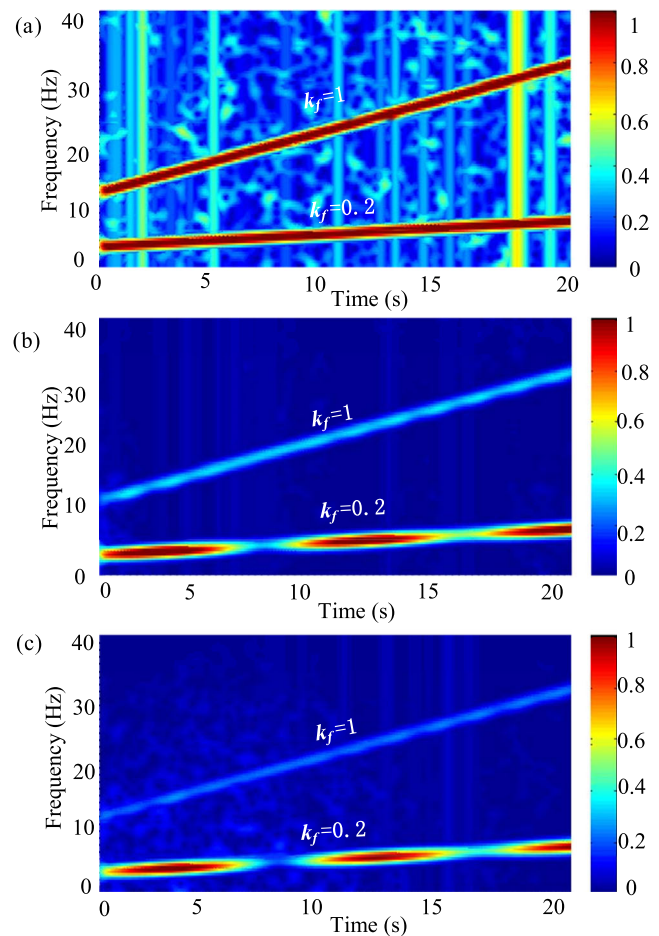


Fig. 5 Time-frequency distributions with respect to a the simulated signal, its outputs via b the NLMS adaptive filter, and c the improved NLMS adaptive filter

filtered out via the preprocessor. This is the reason why the harmonics and inter-harmonics of a thin-walled workpiece should be weakened significantly compared with the chatter frequency.

In order to test the real-time performance of the adaptive signal predictor, we conducted a simulation study with a test signal, which was expressed as

$$x(t) = \sin(0.2\pi t) + 0.4\text{rand}(t) \quad (31)$$

where $\text{rand}(t)$ was a white Gaussian noise. The number of sampling points was 100 in the simulation. The parametric values of the adaptive signal predictor were selected as follows: $N = 5$, $D = 1$. The convergence factor $\mu_0 = 0.001$ was employed in the NLMS algorithm. For the proposed convergence factor, $I = 1$ and $\alpha = 0.001$ were set. The simulation was implemented with MATLAB on an Intel 3.2-GHz computer. The simulation results demonstrate that the execution time for simulated signals processed by the NLMS and improved NLMS adaptive filter is 3.43 ms

and 3.40 ms, respectively. We see that these algorithms are very efficient and show good real-time performance. Moreover, a fast implementation of LMS adaptive filters can also be used to accelerate the computation [37].

5 Experimental results and discussion

Thin-walled parts contain various types, such as the cylindrical and the plate. The experimental workpiece was a thin-walled disc with a stepped surface, which had the 120-mm inner diameter and 180-mm outer diameter. The unmachined disc had a thickness of 7 mm and its material was AISI 4340. End-face turning experiments were performed on a CK6150A lathe. The type of cutter insert was Sumitomo 2NC-DCGW11T304. The oil-based cutting fluid was used to remove heat rapidly and lubricate the chip-tool interface. The experimental setup is shown in Fig. 6. Audio signals were measured by a BSWA MPA 201 microphone with the frequency response of 20~20,000 Hz, which was placed close to the workpiece. Experimental signals were sampled by a HRU-1213 data acquisition system with a maximum sampling rate of 100 kHz.

5.1 Chatter detection scheme based on the WPE

It is mentioned that chatter occurrence leads to the progressive aggregation of energy at a certain frequency. The randomness index has been used as chatter indicators, such as the approximate entropy [38] and energy entropy [17]. Due to high computational efficiency, our attentions are attracted by the WPE that reflects the randomness of energy distribution in the frequency domain. Moreover, it has been proved to be an effective chatter indicator in turning [20]. The definition of the WPE will be subsequently presented. The signal $s(t)$ is decomposed at

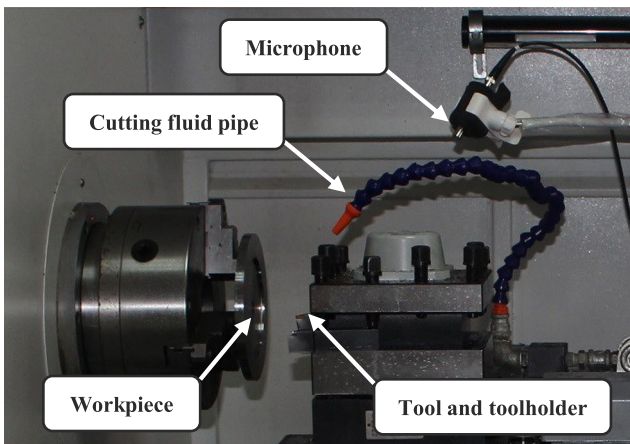


Fig. 6 Experimental setup

the j th level and 2^j vectors of wavelet packet coefficients corresponding to all nodes of the wavelet packet tree are obtained. The wavelet sub-signal in the n th node at the j th level s_j^n is represented as

$$s_j^n(t) = \sum_{k=1}^K d_{j,k}^n \psi_{j,k} \quad (32)$$

where j , n , and k denote the scale level, the node index, and the shift index, respectively, K is the decomposition factor length of the space, $d_{j,k}^n$ is the wavelet packet coefficient, and $\psi_{j,k}$ is the wavelet function. The wavelet packet node energy can represent the signal energy in a certain frequency band and is defined as the square sum of all frequency decomposition coefficients of each node. The energy of the n th node at the j th scale is expressed as

$$E_j^n = \sum_{k=1}^K |d_{j,k}^n|^2 \quad (33)$$

Then the total energy of a signal is obtained by accumulating energy of all sub-bands:

$$E_j = \sum_{n=0}^{2^j-1} E_j^n. \quad (34)$$

To facilitate comparison, the wavelet packet node energy (WPNE) at a certain decomposition level is normalized as

$$p_n = \frac{E_j^n}{E_j}. \quad (35)$$

In order to avoid operating large numbers, the energy vector $V = [E_j^0, E_j^1, \dots, E_j^{2^j-1}]$ is normalized as

$$\begin{aligned} V^n &= [p_0, p_1, \dots, p_{2^j-1}] \\ &= \frac{1}{E_j} [E_j^0, E_j^1, \dots, E_j^{2^j-1}]. \end{aligned} \quad (36)$$

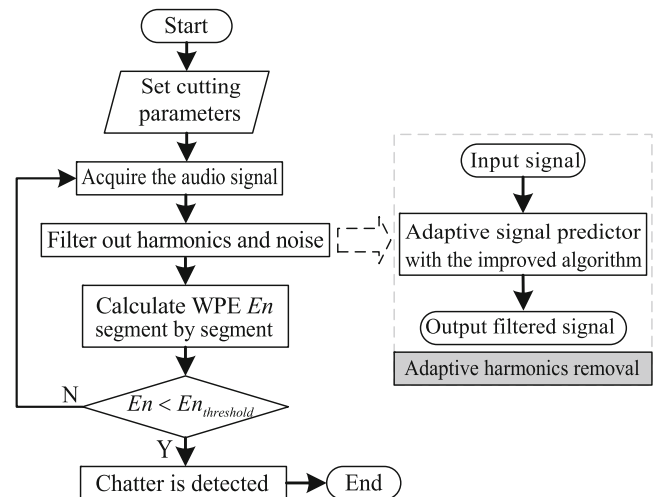


Fig. 7 Flowchart of the proposed chatter detection scheme with the WPE

Finally, the WPE is calculated as

$$En = - \sum_{n=0}^{2^j-1} p_n \ln p_n. \tag{37}$$

When the WPE is used as the chatter indicator, the flowchart of the proposed chatter detection scheme is shown in Fig. 7. The sound in the turning process is on-line captured by a microphone. The harmonics of the natural frequency of workpieces and noise are filtered out through the adaptive signal predictor with the NLMS or improved NLMS algorithm. The filtered signal is utilized to calculate the WPE value, which is compared with the predefined threshold. When the WPE is below the set threshold, chatter is thought to occur. The threshold value for chatter detection is experimentally determined.

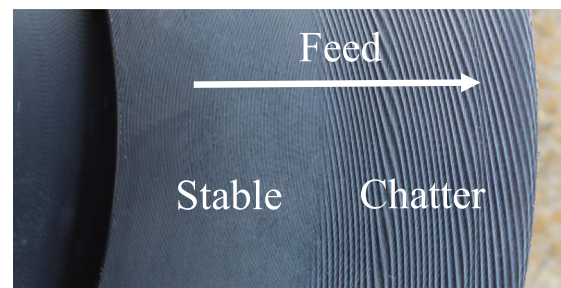
5.2 Experimental verification

To determine its effectiveness and adaptability, the proposed method was applied to experimental signals recorded under different cutting conditions. Experiment 1 was illustrated to testify the validity of the proposed method in harmonics and noise removal. The cutting parameters for Experiment 1 are listed in Table 1. The audio signal was sampled at 40 kHz. The machined surface of the workpiece and collected signals are shown in Fig. 8a and b, respectively. The audio signal in Fig. 8a is divided into three stages, which are the stable stage, transition stage, and chatter stage according to the amplitude. To reveal the presence of harmonics, the FFT spectrum of audio signals in the transition state is provided in Fig. 8c.

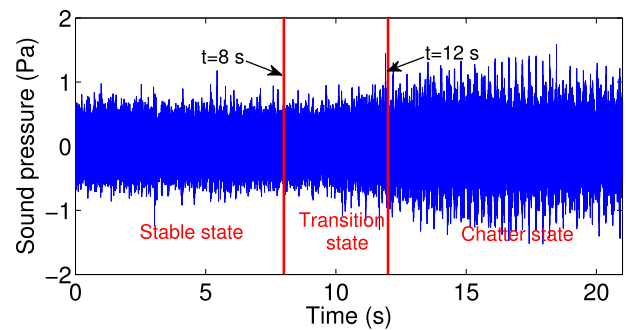
In Fig. 8b, the machining process is stable before t reaches 8 s, then chatter starts to develop and arrives at the fully developed stage at around $t = 12$ s. It is reasonable that chatter vibration is induced during the turning process since the thin-walled disc has a decreasing rigidity when the tool tip moves towards the edge. On the other hand, the harmonics and inter-harmonics of natural frequencies of thin-walled discs are excited easily due to low modal frequencies. In Fig. 8c, the natural frequency and its harmonics can be clearly observed. These emerging harmonics disturb conventional energy distribution in the premature stage, and thereby degrade the effectiveness of existing chatter detection methods. To solve this problem, the adaptive filtering approach is utilized to filter out harmonics.

Table 1 Cutting parameter setting for experiments

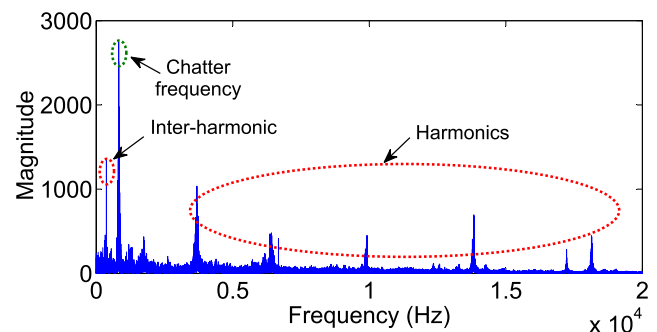
	Spindle speed (r/min)	Feed rate (mm/r)	Depth of cut (mm)
Exp. 1	300	0.12	0.2
Exp. 2	250	0.1	0.16



(a)



(b)



(c)

Fig. 8 Finished surface, audio signals, and audio spectrum in Experiment 1: **a** machined surface, **b** audio signals, **c** FFT spectrum of signals ranging from 9.5 to 12 s

The adaptive signal predictor is applied to the audio signal shown in Fig. 8c. The following parametric values in the adaptive signal predictor are selected: $N = 5$, $D = 1$. The NLMS algorithm is implemented with $\mu_0 = 0.005$. In addition, the proposed convergence factor with $\alpha = 0.005$ and $I = 1$ are used in the improved NLMS algorithm. The FFT spectrum of the signal in the transition state and its output via the NLMS and improved NLMS adaptive filter are plotted in Fig. 9a.

In Fig. 9a, the harmonics of the natural frequency and random noise are effectively removed through the NLMS adaptive filtering. When the improved NLMS algorithm substitutes for the NLMS one, magnitudes of the harmonics further decrease and random noise is canceled more thoroughly. Meanwhile, the amplitude

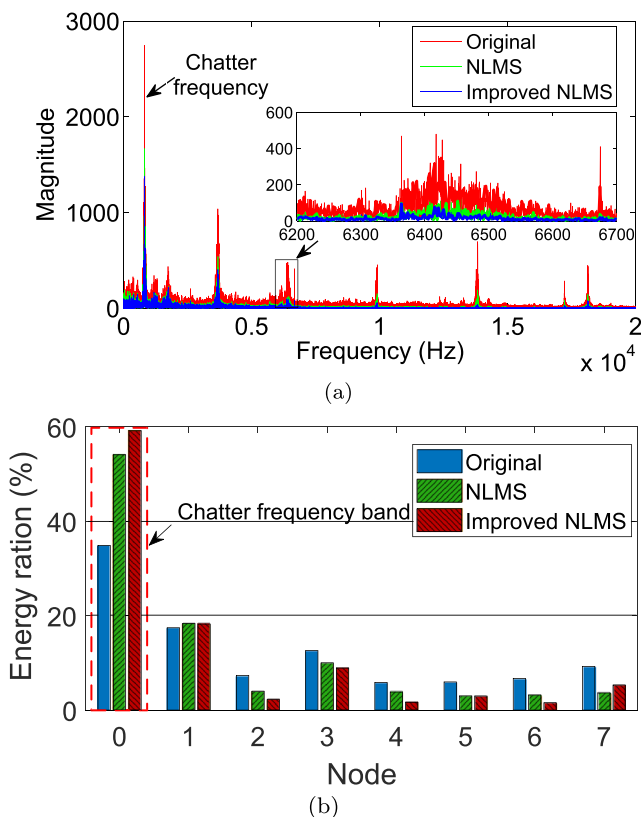


Fig. 9 Experimental result comparisons with different preprocessing methods for Experiment 1: **a** FFT spectrum, **b** percentages of the WPNE for the signal in Fig. 8c and its output via the NLMS and improved NLMS adaptive filter

drop of the chatter frequency can also be seen after preprocessing. But the amplitude of chatter frequency exhibits less relative reduction compared with that of the harmonics. The preprocessed audio signals have a similar energy distribution with conventional signals in turning. Therefore, chatter detection methods based on the spectral characteristics of signals can be effective again.

In Experiment 1, the dominant natural frequency and damping ratio of the disc obtained by modal tests are 813.8 Hz and 0.01, respectively. The chatter frequency in Experiment 1 is 822 Hz, which is recognized by the FFT spectrum of signals in chatter state. According to Eq. 20, we delineate the function curve with respect to f_c and f_n , the slope of whose fitting straight line is 0.2. In other words, the change rate of the chatter frequency is 0.2 times that of the dominant natural frequency, which explains the reason for the harmonics removal in Fig. 9a.

The WPNE is calculated to quantitate the effect of the adaptive filtering approach. Because energy concentration around the natural frequency is a significant characteristic of chatter occurrence, the percentage of WPNE in chatter frequency band can be viewed as a chatter indicator. The size of each frequency band is 2500 Hz at the

third level of wavelet packet decomposition of signals. Therefore, the chatter frequency of 822 Hz in Experiment 1 is located in the first frequency band ranging from 0 to 2500 Hz. The percentages of the third level WPNE for three signals in Fig. 9a are shown in Fig. 9b. It is noted that the WPNE percentage of the chatter frequency band increases by approximately 20% after the signal in the transition state is processed with the NLMS adaptive signal predictor. This percentage is further enhanced by almost 5% if we use the improved NLMS algorithm instead. Therefore, the preprocessing procedure is able to highlight

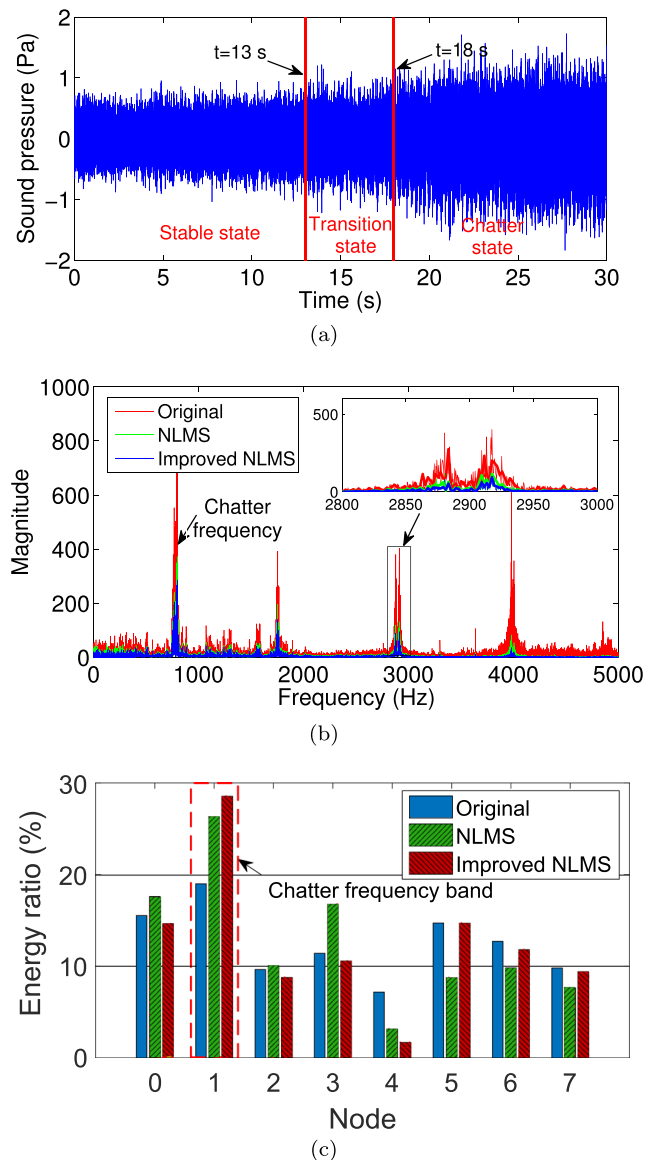


Fig. 10 Experimental result comparisons with different preprocessing methods for Experiment 2: **a** audio signals, **b** FFT spectrum of the original signal ranging from 13 to 15.5 s and its output via the NLMS and improved NLMS adaptive filter, **c** percentages of the WPNE for three signals in Fig. 10b

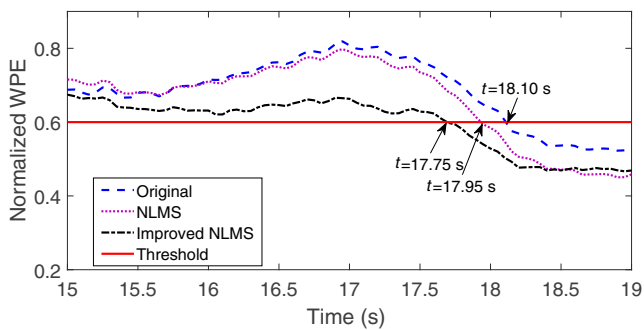


Fig. 11 Normalized WPEs of the signal at the transition stage for Experiment 2 and its output via the NLMS and improved NLMS adaptive filter

the characteristics of energy concentration at the transition stage, which benefits the early detection of chatter.

5.3 Case study

To reduce the effect of harmonic interference, the proposed filtering method is added into the conventional chatter detection system as a preprocessing step in turning of thin-walled parts. A case study for chatter detection named Experiment 2 was conducted to investigate the influence of the preprocessor. It should be noted that the signal in Experiment 2 originated from different cutting stages with Experiment 1. In other words, the workpieces in the two experiments had different thicknesses. Experiment 2 was performed with cutting parameters listed in Table 1 and the sampling frequency was changed to 10 kHz. Experimental results are presented in Fig. 10. The audio signal provided in Fig. 10a is segmented into three stages, namely, stable stage, transition stage, and chatter stage. FFT spectra of the original signal and processed signals through the NLMS and improved NLMS adaptive signal predictor are illustrated in Fig. 10b. The following parametric values in the adaptive signal predictor are selected: $N = 10$, $D = 10$, and other parameters are the same as Experiment 1.

The FFT spectrum of the original signal shows that the chatter frequency is 783 Hz in Experiment 2. It is observed that harmonics and noise have reduced dramatically after being processed by the NLMS adaptive signal predictor in Fig. 10b. Furthermore, the improved NLMS algorithm enhances the ability of the adaptive filtering method to remove harmonics and noise. The chatter frequency component also attenuates slightly due to its slowly time-varying frequency. But we can see that the amplitude of chatter frequency shows less relative reduction compared with the natural frequency and its harmonics. In addition, Fig. 10c presents the percentages of the third level WPNE for three signals in Fig. 10b. It is worth noting that the chatter frequency of 783 Hz is located in the second

frequency band, which ranges from 626 to 1250 Hz. The WPNE percentage of the chatter frequency band increases by 7.3% through the preprocessor with the NLMS filter. Besides, this percentage is further enhanced by almost 2% if the NLMS algorithm is replaced with the improved one. Consequently, the energy aggregation characteristics caused by chatter can be captured as early as possible when adding the adaptive filtering step.

To reveal the effect of the proposed method on chatter detection, we compare the test results for chatter detection with and without preprocessing using the signal of Experiment 2. The sliding window with 50% overlap was utilized to calculate the WPE and its length is 2000 samples. The third level of the wavelet packet decomposition and the Daubechies wavelet (db3) were selected for the computation of the WPE. The parameter setting of the adaptive signal predictor was identical to that used in Experiment 1. Besides, the WPE value is normalized by divided the maximum value of the WPE and the threshold of the normalized WPE is set to 0.6. Figure 11 shows normalized WPEs of the original signal at the transition stage and its output via the NLMS and improved NLMS adaptive filter. In Fig. 11, normalized WPEs of the original signal and its output via the NLMS and improved NLMS adaptive filter drop below the threshold at $t = 18.10$ s, $t = 17.95$ s and $t = 17.75$ s, respectively. In other words, chatter is detected using the normalized WPEs of preprocessed signals by the NLMS and improved NLMS adaptive signal predictor earlier than that of the original signal by 0.15 s and 0.35 s, respectively. As a result, those detrimental effects induced by chatter would be remarkably reduced.

6 Conclusions

The emergence of harmonics of the natural frequency in the flexible workpiece turning process changes conventional frequency distribution patterns in the development of chatter, and further vitiates the detection of chatter. The time-dependence and uncertainty in the dynamic characteristics of the flexible workpiece make the identification of the natural frequency more difficult. In this paper, an adaptive harmonics removal approach for chatter detection is proposed to simultaneously remove harmonics and noise from the measured signal in turning of thin-walled workpieces. Simulation and experimental results showed that the proposed adaptive harmonics removal approach could alleviate the interference of harmonics and noise in the case of no prior knowledge. The main contributions of this paper are concluded as follows:

1. The investigation into signal frequencies during the turning of thin-walled workpieces was firstly conducted

and discovered that the rate of change of the chatter frequency was much slower than that of the natural frequency.

2. Based on the aforementioned finding, the adaptive signal predictor is introduced as a preprocessor to remove the harmonics and noise but remain the chatter frequency component. Moreover, an improved NLMS algorithm is put forward to enhance the filtering ability.
3. The simulations demonstrated that the adaptive signal predictor was capable to filter out signal components with large rates of frequency change and very efficient in terms of the computation time.
4. The turning experiments of thin-walled discs were conducted to validate the effectiveness of the proposed method. Experimental results showed that the harmonics of the natural frequency and noise were significantly attenuated through the preprocessor with the NLMS algorithm. Moreover, the improved NLMS algorithm outperformed the NLMS one in the filtering performance. Besides, chatter was recognized earlier when adding the preprocessing step for harmonics removal in chatter detection.

Funding information This research was financially supported in part by the Program of Shanghai Subject Chief Scientist (18XD1401700), the National Basic Research Program of China (2013CB035804).

References

1. Liu Y, Wang X, Lin J, Zhao W (2016) Early chatter detection in gear grinding process using servo feed motor current. *Int J Adv Manuf Technol* 83:1801–1810
2. Siddhpura M, Paurobally R (2012) A review of chatter vibration research in turning. *Int J Mach Tool Manuf* 61:27–47
3. Ma L, Melkote SN, Castle JB (2013) A model-based computationally efficient method for on-line detection of chatter in milling. *J Manuf Sci Eng* 135(3):031007
4. Caliskan H, Kilic ZM, Altintas Y (2018) On-line energy-based milling chatter detection. *J Manuf Sci Eng* 140(11):111012
5. Meng HF, Kang Y, Chen Z, Zhao Y, Liu G (2015) Stability analysis and stabilization of a class of cutting systems with chatter suppression. *IEEE/ASME Trans Mechatronics* 20(2):991–996
6. Ding L, Sun Y, Xiong Z (2018) Online chatter suppression in turning by adaptive amplitude modulation of spindle speed variation. *J Manuf Sci Eng* 140(12):121003
7. Tuysuz O, Altintas Y (2017) Frequency domain updating of thin-walled workpiece dynamics using reduced order substructuring method in machining. *J Manuf Sci Eng* 139(7):071013
8. Mehdi K, Rigal J-F, Play D (2002) Dynamic behavior of a thin-walled cylindrical workpiece during the turning process, part 1: Cutting process simulation. *J Manuf Sci Eng* 124(3):562–568
9. Khoshdarregi MR, Altintas Y (2018) Dynamics of multipoint thread turning-part II: application to thin-walled oil pipes. *J Manuf Sci Eng* 140(4):041016
10. Liu Y, Wu B, Ma J, Zhang D (2016) Chatter identification of the milling process considering dynamics of the thin-walled workpiece. *Int J Adv Manuf Technol* 89(5-8):1765–1773
11. Urbikain G, López de Lacalle LN, Campa FJ, Fernández A, Elías A (2012) Stability prediction in straight turning of a flexible workpiece by collocation method. *Int J Mach Tool Manuf* 54:73–81
12. Lauro CH, Brandão LC, Baldo D, Reis RA, Davim JP (2014) Monitoring and processing signal applied in machining processes—A review. *Measurement* 58(58):73–86
13. Tony LS (2003) Chatter recognition by a statistical evaluation of the synchronously sampled audio signal. *J Sound Vib* 262(3):721–730
14. Eynian M, Altintas Y (2009) Chatter stability of general turning operations with process damping. *J Manuf Sci Eng* 131(4):041005
15. Kuljanic E, Totis G, Sortino M (2009) Development of an intelligent multisensor chatter detection system in milling. *Mech Syst Signal Process* 23(5):1704–1718
16. Chen Y, Li H, Jing X, Hou L, Bu X (2019) Intelligent chatter detection using image features and support vector machine. *Int J Adv Manuf Technol* 102(5-8):1433–1442
17. Liu C, Zhu L, Ni C (2018) Chatter detection in milling process based on VMD and energy entropy. *Mech Syst Signal Process* 105:169–182
18. Cao H, Zhou K, Chen X (2015) Chatter identification in end milling process based on EEMD and nonlinear dimensionless indicators. *Int J Mach Tool Manuf* 92:52–59
19. Yao Z, Mei D, Chen Z (2010) On-line chatter detection and identification based on wavelet and support vector machine. *J Mater Process Tech* 210(5):713–719
20. Sun Y, Xiong Z (2016) An optimal weighted wavelet packet entropy method with application to real-time chatter detection. *IEEE/ASME Trans Mechatronics* 21(4):2004–2014
21. Jia G, Wu B, Hu Y, Xie F, Liu A (2013) A synthetic criterion for early recognition of cutting chatter. *Sci China Tech Sci* 56(11):2870–2876
22. Stepan G, Kiss AK, Ghalamchi B, Sopanen J, Bachrathy D (2017) Chatter avoidance in cutting highly flexible workpieces. *CIRP Ann-Manuf Techn* 66:377–380
23. Arnab C, Dwivedy SK (2018) Nonlinear dynamic analysis of flexible workpiece and tool in turning operation with delay and internal resonance. *J Sound Vib* 434:358–378
24. Guo J, Lee KM, Liu W, Bo W (2015) Design criteria based on modal analysis for vibration sensing of thin-wall plate machining. *IEEE/ASME Trans Mechatronics* 20(3):1406–1417
25. Lu K, Lian Z, Gu F, Liu H (2018) Model-based chatter stability prediction and detection for the turning of a flexible workpiece. *Mech Syst Signal Process* 100:814–826
26. Taylor CM, Turner S, Sims ND (2010) Chatter, process damping, and chip segmentation in turning: A signal processing approach. *J Sound Vib* 329(23):4922–4935
27. Turkes E, Orak S, Neseli S, Yaldiz S (2011) Linear analysis of chatter vibration and stability for orthogonal cutting in turning. *Int J Refract Met H* 29(2):163–169
28. Altintas Y (2012) *Manufacturing automation: metal cutting mechanics, machine tool vibrations and CNC design*, 2nd edn. Cambridge University Press, New York
29. Gerasimenko A, Guskov M, Duchemin J, Lorong P, Gousskov A (2015) Variable compliance-related aspects of chatter in turning thin-walled tubular parts. *Procedia CIRP* 31:58–63
30. Tang A, Liu Z (2009) Three-dimensional stability lobe and maximum material removal rate in end milling of thin-walled plate. *Int J Adv Manuf Technol* 43(1):33–39
31. Han B, Bae B, Ovaska SJ (2005) Reference signal generator for active power filters using improved adaptive predictive filter. *IEEE Trans Ind Electron* 52(2):576–584

32. Rosado-Munoz A, Bataller-Mompean M, Soria-Olivas E, Scarante C, Guerrero-Martinez J (2011) FPGA implementation of an adaptive filter robust to impulsive noise: two approaches. *IEEE Trans Ind Electron* 58(3):860–870
33. Matthew OTC, Theeraphong W (2013) A direct method of adaptive FIR input shaping for motion control with zero residual vibration. *IEEE/ASME Trans Mechatronics* 18(1):316–327
34. Wang C, Zhang X, Cao H, Chen X, Xiang J (2018) Milling stability prediction and adaptive chatter suppression considering helix angle and bending. *Int J Adv Manuf Technol* 95(9):3665–3677
35. Diniz PS (2013) Adaptive filtering: algorithms and practical implementation. Springer, New York
36. Bismor D, Czyz K, Ogonowski Z (2016) Review and comparison of variable step-size LMS algorithms. *J Vib Acoust* 21(1):24–39
37. Ferrara E (1980) Fast implementations of LMS adaptive filters. *IEEE Trans Acoust Speech Signal Process* 28(4):474–475
38. Pérez-Canales D, Vela-Martínez L, Jáuregui-Correa JC, Alvarez-Ramirez J (2012) Analysis of the entropy randomness index for machining chatter detection. *Int J Mach Tool Manuf* 62(1):39–45

Publisher's note Springer Nature remains neutral with regard to jurisdictional claims in published maps and institutional affiliations.